Diamond & Related Materials 108 (2020) 107961

Contents lists available at ScienceDirect

Diamond & Related Materials

journal homepage: www.elsevier.com/locate/diamond

Mechanical and thermal properties of ZnO anchored GO reinforced phenol formaldehyde resin

P.K. Sandhya[a], M.S. Sreekala[b,*], Moothetty Padmanabhan[a,c], Sabu Thomas[a]

[a] School of Chemical Sciences, Mahatma Gandhi University, Kottayam 686560, Kerala, India
[b] Post Graduate Research Department of Chemistry, Sree Sankara College, Kalady 683574, Kerala, India
[c] Department of Chemistry, Amrita Vishwa Vidyapeetham, Amritapuri, 690525, Kerala, India

ARTICLE INFO

Keywords:
Phenol formaldehyde
ZnO-RGO
Nanocomposites
Fracture mechanism

ABSTRACT

Phenol formaldehyde/ZnO-decorated graphene oxide (PF/ZnO-RGO) nanocomposites were prepared by solution mixing method. The ZnO-RGO nanofillers were prepared by decorating ZnO particles on the surface of graphene oxide (GO) and it is interesting that the reduction of GO to RGO and conversion of ZnO to nano ZnO occur simultaneously. The ZnO-RGO nanofiller can improve the mechanical and thermal properties of PF resin by the action of synergetic effect between the metal oxide and graphene sheets. The structural properties and morphology of the nanocomposites were studied by X-ray diffraction (XRD) and high resolution transmission electron microscope (TEM) respectively. The effect of ZnO-RGO on the mechanical properties of the nanocomposites were studied by tensile and Izod impact tests. Scanning electron microscopy (SEM) images were used to study the fracture mechanism of the nanocomposites. The thermal properties of the nanocomposites were studied using thermogravimetric analysis (TGA) and the activation energy of decomposition was evaluated by Coats Redfern and Broido's method.

1. Introduction

Graphene based polymer nanocomposites has become an important research area due to its applications in various fields and their ability to improve mechanical, thermal, electrical, and other multifunctional properties of the polymer matrix even in low filler content. Due to van der Waals and π-π stacking interaction graphene sheets undergo re-stacking and form agglomerates, which can be solved by anchoring graphene sheets with nanoparticles or using surfactants [1]. Graphene oxide (GO) is a two dimensional carbon nanomaterial and act as a precursor material for the cost-effective and large scale production of graphene-based materials [2]. GO-inorganic nanocomposites and GO-metal oxide nanocomposites received more attention of the researchers due to the charge transfer as well as electronic interaction between GO and attached metal oxide nanoparticle [3]. The enhanced properties and improved performance of the metal compounds can be brought through the electron transport channel of GO. These GO-metal oxide composites preserve both the favorable properties of metal oxide and GO and enhance the intrinsic properties that arise from the synergetic effect between them. Metal-oxide based nanomaterials found a wide range of applications in various fields such as solar cells, super capacitors, biosensors, fuel cells etc. due to their excellent mechanical, electrical, optical, magnetic properties [4]. Recently, ZnO nanostructures with different morphologies were successfully attached to graphene derivatives such as GO or reduced graphene oxide (RGO) [5]. The agglomeration and the stacking of graphene sheets can be prevented by the successful intercalation of metal oxides [3].

Phenol formaldehyde resin (PF) is an excellent thermosetting resin and is widely used in the fields of composites, aerospace, thermal insulation material, structural adhesives, tunnel materials, coatings and so on [6,7]. Most of these applications were made because of its advantages such as excellent heat and cold resistance, thermal and chemical resistance, low cost, excellent ablative property, simple equipment and production technologies, dimensional stability and smoke resistance [8,9]. Inherent brittleness, large volumetric shrinkage during curing and low char yield limits the applications of PF in various fields. At present researchers are interested in improving the properties of phenolic resins by various methods such as reinforcing the PF matrix with nanofillers, use of elastomers, copolymerization, blending and introduction of functional groups with high carbon content [10,11].

There are different GO-metal oxide nanofillers such as GO-ZnO [12,13], GO-CuO[14,15], GO-TiO_2 [16,17] and GO-Fe_3O_4 [18,19] have been reported and studied their potential applications in various fields like energy storage and conversion, catalysis and sensors. But, there are

* Corresponding author.
E-mail address: sreekalams@yahoo.co.in (M.S. Sreekala).

https://doi.org/10.1016/j.diamond.2020.107961
Received 6 February 2020; Received in revised form 30 May 2020; Accepted 31 May 2020
Available online 06 June 2020
0925-9635/

few research articles regarding GO-metal oxide as nanofillers in polymer nanocomposites. Li and colleagues [20] successfully grafted polyether amine on the surface of graphene nanosheets decorated by zinc hydroxystannate boxes, incorporated into epoxy resin and studied the flame-retardant property. They found that the resultant epoxy composites showed superior flame-retardant property due to the excellent processability and good compatibility of graphene organic hybrid material. Huang et al.[3] prepared graphene oxide loaded with ZnO nanoparticles and mixed with poly(lactic acid) by solution blending method. They found that the prepared nanocomposites showed increased tensile strength, a significant enhancement in storage modulus and glass transition temperature. The prepared nanocomposites also exhibit strong ultraviolet resistance and antimicrobial properties at very low loading of the nanofiller. Huang and co-workers [2] fabricated reduced graphene oxide-zinc oxide/cyanate ester/bismaleimide resin nanocomposites by blending method. The mechanical properties, thermal stability, flexural and impact strengths of the composites were enhanced by the addition of filler. Deshmukh and colleagues [21] prepared polymer/inorganic nanocomposites based on hydroxypropyl methylcellulose (HPMC) and polyvinyl alcohol (PVA) as polymer matrix and a combination of graphene oxide and ZnO nanoparticles as fillers using colloidal processing technique. They investigated the morphological, mechanical, and dielectric properties of the nanocomposites and found an enhancement in mechanical and dielectric properties. The enhancement in mechanical properties was due to the homogeneous dispersion of the nanofillers and the strong interfacial interaction between all the components.

In our previous work, ZnO decorated graphene oxide is formed from GO by chemically decorating its surface with ZnO nanoparticles [22] was reported. In this method, both the reduction of GO to RGO and the conversion of ZnO to nano ZnO occur simultaneously. Herein, we develop PF/ZnO-RGO nanocomposites by reinforcing ZnO-RGO nanofillers into PF resin by simple solution mixing method followed by compression moulding. The structural, morphological and mechanical properties of the nanocomposites were studied. The thermal stability, kinetic and thermodynamic parameters of the nancomposites were also determined.

2. Experimental

2.1. Materials

Graphite powder, sodium nitrate ($NaNO_{3)}$, concentrated sulphuric acid (conc. H_2SO_4), potassium permanganate ($KMnO_4$), hydrogen peroxide (H_2O_2), *N*, *N*-dimethylformamide (DMF), zinc acetate dihydrate ($Zn(CH_3COO)_2.2H_2O$) were purchased from Merck, India.

2.2. Preparation of the PF/ZnO-RGO polymer nanocomposites

The nanofiller ZnO decorated graphene oxide were prepared using zinc acetate dehydrate and graphene oxide in DMF solution, heating at 95 °C for 5 h. The detailed method of preparation and characterization of the nanofiller were explained in our research article published elsewhere [22]. The quantity of ZnO-RGO required for the preparation of nanocomposites were taken on the basis of the solid content of PF resin, wet with acetone and stirred well using a mechanical stirrer for 2 h and sonicated for 1 h at 60 °C. The mixture was transferred into tray and kept in an oven at 50 °C until a semi-solid stage is attained, then compression moulded at 100 °C for 30 min. The samples were cut into required size and can be used for further investigation after cooling.

2.3. Characterization of PF/ZnO-RGO nanocomposites

The synthesized solid materials were subjected to powder X-ray diffraction (XRD) analysis using XPERT-PRO X-ray diffractometer using a Ni-filtered Cu K_α radiation ($\theta = 1.5406$ Å) and an operating voltage of 45 kV and a filament current of 35 mA. The High-Resolution Transmission Electron Microscope JEM-2100HRTEM was used to study the morphology of the nanocomposites. The TEM images of PF/ZnO-RGO nanocomposites were obtained by employing ultra-microtome cutting and collected on a 200 mesh Cu grid. The scanning electron microscope JEOL JSM-820 model was used to investigate the surface morphology of the tensile fracture surfaces of nanocomposites, after being coated in a thin gold layer. The tensile properties of the nanocomposites were analyzed using Tinius Olsen universal tensile testing machine according to ASTM D638. Rectangular shaped samples with gauge length of 60 mm were used for conducting the tensile strength with a cross head speed of 2 mm/min. The izod impact strength of the samples was performed using Zwick/Roell HIT 25 P model impact tester according to ASTM D256. The thermo gravimetric analysis (TGA) of the samples were carried out with Perkin Elmer STA 6000 (Simultaneous Thermal Analyzer) at a heating rate of 20 °C per minute under nitrogen atmosphere. The amount of the samples used for analysis varies from 5 to 10 mg and the thermograms were recorded from room temperature to 700 °C.

3. Results and discussions

3.1. Structural analysis of PF/ZnO-RGO nanocomposites by XRD

The XRD data of PF/ZnO-RGO nanocomposites with varying wt% of ZnO-RGO is shown in Fig. 1. From the XRD of ZnO-RGO (inset Fig. 1), it is clear that ZnO-RGO possess high crystallinity with major peak (101) observed at $2\theta = 36.48°$ [22]. But in the case of nanocomposites with

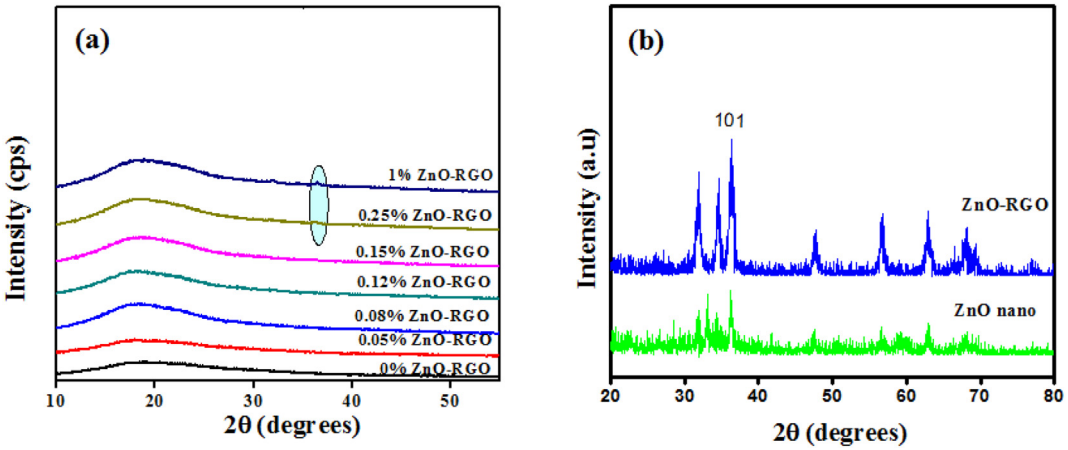

Fig. 1. XRD spectra of (a) neat PF and PF/ZnO-RGO nanocomposites (b) ZnO nano and ZnO-RGO.

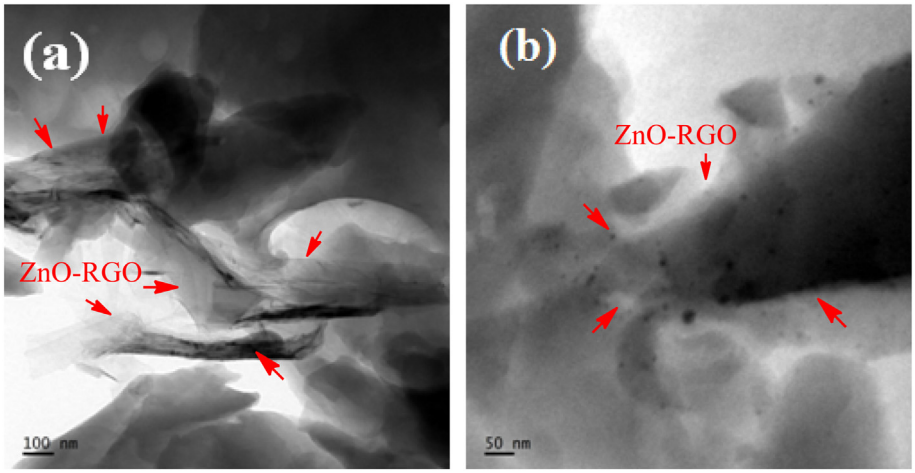

Fig. 2. TEM images of PF/ZnO-RGO nanocomposites with 0.12 wt% ZnO-RGO. Scale bar (a) 100 nm (b) 50 nm.

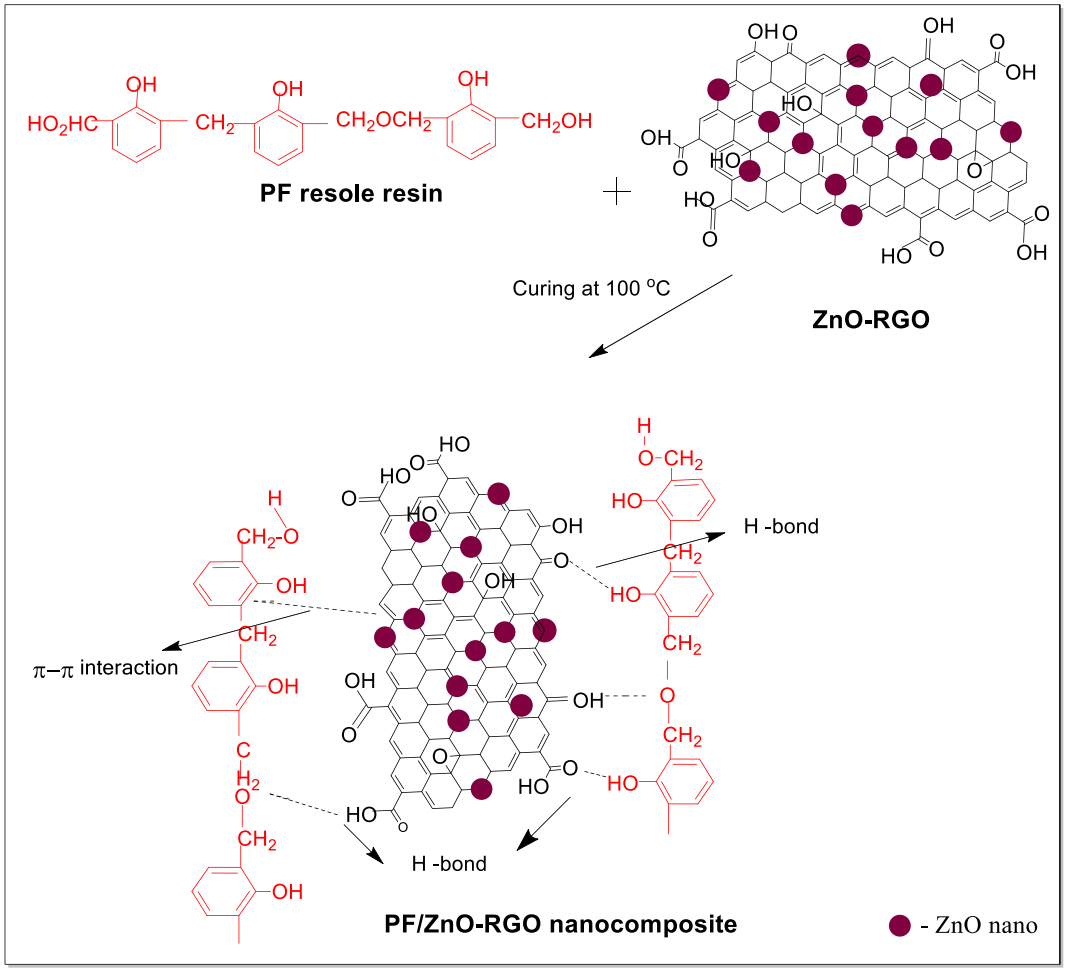

Scheme 1. Schematic representation of interactions present in PF/ZnO-RGO nanocomposites.

lower wt% of ZnO-RGO, there was no such peak is observed, indicating that no change is produced in the crystallinity of samples. But, at higher wt% of ZnO-RGO, the peak corresponding to $2\theta = 36.48^{\circ}$ is observed. From this it is clear that the dispersion of ZnO-RGO in PF was influenced by the amount of ZnO-RGO.

3.2. Morphology of PF/ZnO-RGO nanocomposites by TEM analysis

The TEM micrographs were employed to characterize the morphology and the dispersion of ZnO-RGO sheets in the PF matrix. Fig. 2 depicts the TEM micrograph of PF/ZnO-RGO nanocomposites with 0.12 wt% ZnO-RGO in two different magnifications. The red arrows in Fig. 2(a) and (b) represent the ZnO-RGO nanosheets. The wrinkled structure of ZnO-RGO sheets can be clearly observed from the TEM

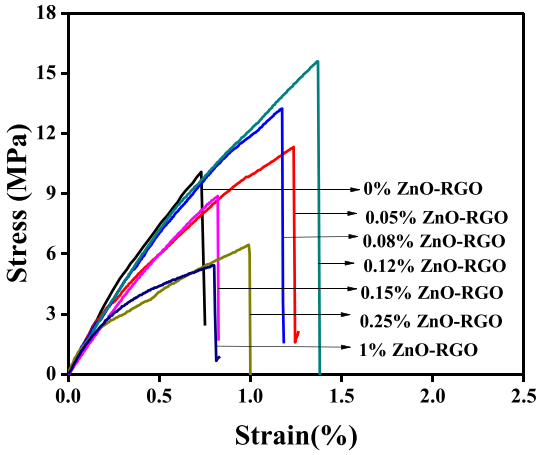

Fig. 3. Stress-strain curves of PF/ZnO-RGO nanocomposites.

image (Fig. 2(a)), however the ZnO nanoparticles attached to RGO sheets can hardly be observed. But in the magnified image (Fig. 2(b)), there are some ZnO nanoparticles are clearly observed on the surface of RGO sheets appeared as dark coloured dots. The wrinkled and overlapped structure of graphene sheets show that single graphenes or stacks of graphene with several nanometers of thickness were dispersed finely in the PF matrix. The ZnO-RGO sheets were dispersed well in PF matrix without any large agglomerates and it can be visualized from the TEM images (Fig. 2).

3.3. Mechanical properties of PF/RGO nanocomposites

H-bonding and π-π interactions are present during the formation of PF/ZnO-RGO nanocomposites and a schematic representation is shown in Scheme 1. The mechanical properties of PF/ZnO-RGO nanocomposites were studied by performing tensile tests of nanocomposites and the stress-strain curves are presented in Fig. 3. The results showed that the addition of ZnO-RGO improved the mechanical properties of PF matrix. An increase in mechanical stress is observed for ZnO-RGO composites up to 0.12 wt% ZnO-RGO due to the effective load transfer between PF and ZnO-RGO sheets. At higher wt% of ZnO-RGO, the aggregation of nanofillers leads to a decrease in mechanical stress.

The tensile strength and tensile modulus of PF/ZnO-RGO nanocomposites are shown in Fig. 4(a) and (b). With the increase in wt% of nanoparticle content the tensile strength increases up to 0.12 wt% of ZnO-RGO and decreases up to 1 wt% of the nanoparticle content. The maximum value of tensile strength is observed for nanocomposites with 0.12 wt% of ZnO-RGO and is about 54% higher than that of neat PF. The increase is due to the presence of ZnO on the surface of GO could

Table 1
Mechanical properties of PF/ZnO-RGO nanocomposites.

ZnO-RGO contents (%)	Tensile strength (MPa)	Young's modulus (MPa)	Elongation at break (%)	Izod impact strength (notched) (kJ/m^2)
0	10.35 ± 0.28	1061 ± 41	0.78 ± 0.05	1.04 ± 0.09
0.05	11.30 ± 0.50	1103 ± 20	0.75 ± 0.05	1.20 ± 0.06
0.08	13.48 ± 0.10	1481 ± 83	0.87 ± 0.04	1.30 ± 0.08
0.12	15.98 ± 0.45	2190 ± 80	2.47 ± 0.27	1.53 ± 0.02
0.15	09.01 ± 0.98	1701 ± 91	2.39 ± 0.01	1.15 ± 0.03
0.25	06.67 ± 0.23	1468 ± 53	1.31 ± 0.09	1.12 ± 0.04
1	05.41 ± 0.35	1134 ± 12	0.93 ± 0.06	1.07 ± 0.03

avoid the re-agglomeration of RGO sheets and the improved dispersion state of nanofiller in the PF matrix. In the studies of Kalali et al. [23] metal oxide decorated RGO reinforced epoxy nanocomposites exhibited high tensile strength than RGO alone. A decrease in the tensile strength is observed for 0.15 to 1 wt% ZnO-RGO nanocomposites due to the clustering or aggregation of the nanoparticles. Here, the interaction between the nanoparticle and the polymer matrix becomes less and the nanoparticle-nanoparticle interactions occur more. The tensile modulus of the nanocomposites shows a similar trend as that of tensile strength. The maximum value of tensile modulus was observed for 0.12 wt% ZnO-RGO (2190 MPa) and it is 107% higher than that of neat PF. This may be due to the better dispersion of ZnO-RGO into the PF matrix and the strong interaction between ZnO-RGO and PF matrix. But at higher wt% of nanoparticle content the tensile modulus gets decreased and it is due to the fact that with increasing amount of RGO in the polymer matrix the aggregation tendency of the ZnO-RGO sheets in the PF matrix occurred [10,24]. The increase in tensile modulus of PF/ZnO-RGO nanocomposites as compared to PF/RGO nanocomposites in our previous work was due to the synergetic effect of ZnO and GO on the PF matrix [25]. The mechanical properties of PF/ZnO-RGO nanocomposites are tabulated in Table 1.

3.4. Tensile fracture mechanism by SEM analysis

The fracture mechanism of the PF/ZnO-RGO nanocomposites can be studied with the help of SEM images. The SEM images clearly showed the highly brittle failure mode without crazing in fracture surface of neat PF indicating fast crack propagation (Fig. 5). Similar nature is observed with PF/ZnO-RGO composites with 0.05 wt% of ZnO-RGO, this low wt% of ZnO-RGO is not sufficient for producing any characteristic changes in the fracture surface of the nanocomposites. But the SEM images of 0.12 wt% of ZnO-RGO are different from that of neat PF. The increase in the roughness of the fracture surface leads to the formation of craze, which is formed as a result of inhibition of crack

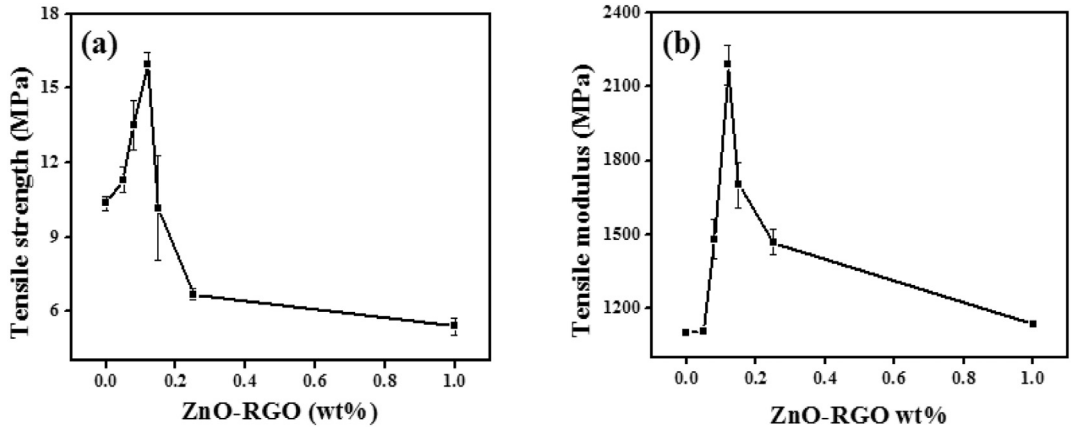

Fig. 4. (a) Tensile strength and (b) tensile modulus of PF/ZnO-RGO nanocomposites.

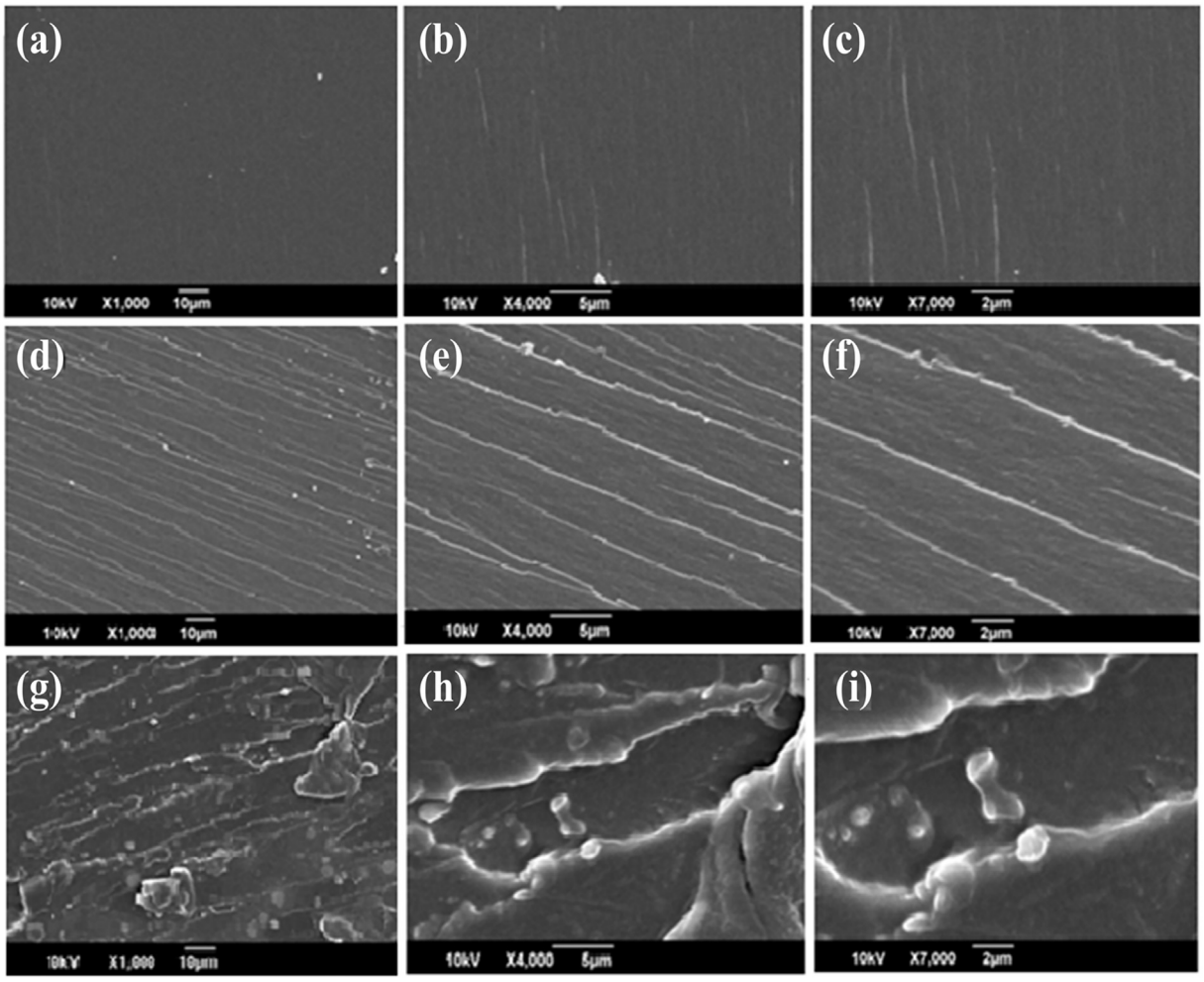

Fig. 5. SEM images of tensile fracture surfaces of PF/ZnO-RGO nanocomposites (Scale bar 10 μm, 5 μm, 2 μm) (a–c) neat PF (d–f) 0.12 wt% ZnO-RGO (g–i) 1 wt% ZnO-RGO.

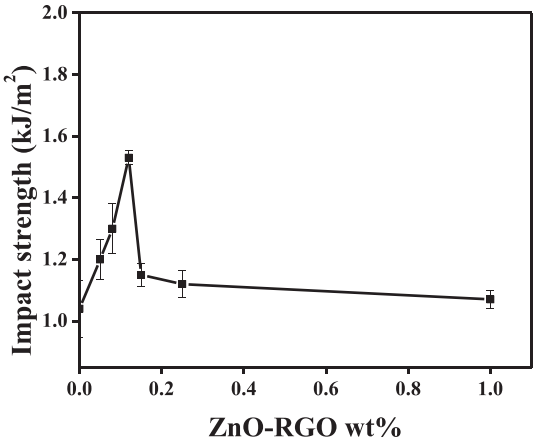

Fig. 6. Impact strength of PF/ZnO-RGO nanocomposites.

propagation by the nanoparticles [26]. This leads to an increase in the toughness of the nanocomposites. In other words, surface roughness increased with increase in ZnO-RGO content indicating that with the introduction of ZnO-RGO into PF resin can absorb energy and the shear yielding gets localized. The presence of rough fracture surface means the larger surface area available for dissipation of energy. The ridges observed on the surface are run parallel to the crack growth direction (Fig. 5(d)–(f)). But, on analyzing the SEM image of the fracture surface of 1 wt% of ZnO-RGO (Fig. 5(g–i)), a marked change is observed. Here, at higher wt% of ZnO-RGO the aggregation of nanoparticle content occurs and restricts the interaction between the matrix and nanofiller content. From the SEM images it is clear that there was no regularity is observed on the fracture surface due to the aggregation of the nanofillers which resulted in the poor interfacial adhesion between ZnO-RGO and PF. This poor interfacial adhesion leads to the stress concentration and resulted in decreased mechanical properties [27].

3.5. Izod impact strength of PF/ZnO-RGO nanocomposites

Fig. 6 represents the impact strength of PF/ZnO-RGO nanocomposites with varying wt% of ZnO-RGO content. From the results, it is clear that the addition of ZnO-RGO into the PF matrix improves the impact strength of PF matrix. The impact strength increases gradually with increase wt% of ZnO-RGO content. The maximum value of impact strength is observed for composites with 0.12 wt% ZnO-RGO and it is 47.11% higher than that of neat PF. The strong interaction that exists between the nanoparticle and the matrix can transfer any part of the external load. There is a decrease in the impact strength, which is observed for nanocomposites at higher wt% of ZnO-RGO due to the poor dispersion and interaction between the nanoparticle and the polymer matrix.

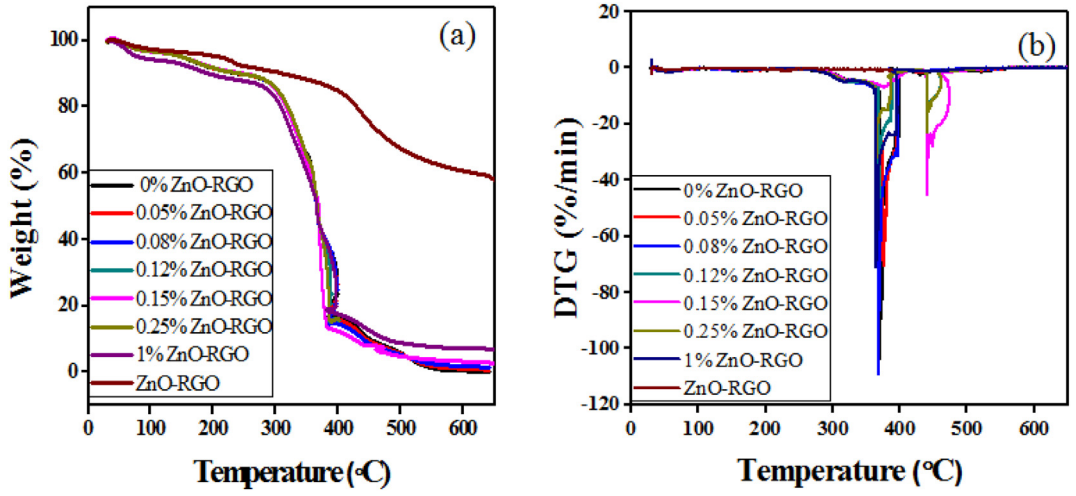

Fig. 7. (a) TGA and (b) DTG curves of PF/ZnO-RGO nanocomposites.

Table 2
Thermal degradation behavior of PF and PF/ZnO-RGO nanocomposites by TGA analysis.

Sample (% ZnO-RGO)	Temperature (°C) at 5% loss (T_5%)	Temperature (°C) at 10% loss (T_{10}%)	Residue at 640 °C	Temperature at maximum degradation rate (°C)
0	150.95	241.39	00.03	372.67
0.05	151.42	245.97	01.50	376.34
0.08	151.83	249.57	02.98	367.35
0.12	125.15	215.61	03.34	370.09
0.15	082.29	194.98	03.71	377.52
0.25	082.08	194.15	05.38	364.93
1	081.79	193.46	07.05	364.84
ZnO-RGO	211.53	311.83	59.20	471.13

Table 3
E_a, ΔS, ΔH, and ΔG values of PF/ZnO-RGO nanocomposites.

Sample (% ZnO-RGO)	E_a (kJ/mol)		ΔS J/Kmol	ΔH kJ/mol	ΔG kJ/mol
	Redfern's method	Broido's method			
0	112.24	122.39	17.20	−5242.48	−16,319
0.05	111.95	122.09	17.18	−5281.18	−16,423
0.08	110.61	120.76	20.06	−2955.17	−10,353
0.12	124.63	134.78	44.54	−2941.16	−19,363
0.15	114.20	124.34	26.23	−3557.43	−15,140
0.25	122.18	132.33	41.61	−2905.20	−18,060
1	127.64	137.78	50.36	−2918.95	−21,372

3.6. TGA of PF/ZnO-RGO nanocomposites

The study of thermal degradation of polymer nanocomposites is one of the main factors to be investigated due to the increase in demand for the usage of nanocomposites. The thermo gravimetric (TGA) curves along with the derivative (DTG) curves of PF/ZnO-RGO nanocomposites are shown in Fig. 7. Table 2 illustrates the temperatures at which 5% and 10 wt% mass loss is observed, the residue at 640 °C and the maximum degradation rate of the nanocomposites. The initial mass loss is due to the evaporation of water vapours and it is observed below 100 °C. The breaking of bond between methylene and benzene occurs below 300 °C. The major mass loss occurs between 350 and 400 °C and is due to the elimination of volatiles [28]. Similar degradation behavior is observed for neat PF and PF/ZnO-RGO nanocomposites which exhibits three stages such as vaporization of water molecules, decomposition of PF network and the oxidation of the char residues. From the Fig. 7, it is clear that the existence of ZnO-RGO didn't significantly alter the degradation mechanism of the PF resin. Similar results were reported in the studies of Cui et al. [29] and Chhetri et al. [30] in epoxy systems. The temperature at 5% and 10% weight loss for neat PF is 150.95 °C and 241.39 °C respectively. The incorporation of 0.05 wt% and 0.08 wt% of ZnO-RGO results in an increase in T_5% and T_{10}%. However, after 0.08 wt% ZnO-RGO, a decrease in the values of T_5% and T_{10}% observes with increase in wt% of ZnO-RGO. From this it is concluded that the thermal stability of PF/ZnO-RGO nanocomposites is dependent on the dispersion of ZnO-RGO in the PF matrix but not relevant to the wt% of ZnO-RGO. The char yield of PF nanocomposites at 640 °C is found to be higher for different wt% of ZnO-RGO than neat PF and is due to the presence of interfacial interaction which restricts the volatilization of the polymer decomposition.

3.7. Determination of kinetic and thermodynamic parameters of PF/ZnO-RGO nanocomposites

The thermal data obtained from TGA analysis was useful for finding the kinetic parameters of PF/ZnO-RGO at the main stage of decomposition. The activation energy of decomposition was evaluated by Coats Redfern and Broido's method using Eqs. (1) and (2).

$$E_a = 2.303\mathrm{R} \times \text{slope} \tag{1}$$

$$\log(-\log(1-\alpha)) = \left(\frac{-E_a}{2.303\,R}\right)\frac{1}{T} + Constant \tag{2}$$

The relation between log (−log (1-α)) and 1/T gives a good approximation to a straight line. The activation energy can be calculated from the plot of log (−log (1-α)) versus 1/T.

The entropy of activation (ΔS), enthalpy of activation (ΔH), and free energy change (ΔG) can be calculated using the following equations [31,32]

$$\Delta S = 2.303\,R\log\left(\frac{Ah}{K_B T_p}\right) \tag{3}$$

$$\Delta H = E - RT_p \tag{4}$$

$$\Delta G = \Delta H - T_p\Delta S \tag{5}$$

where, A is the pre-exponential factor, K_B is the Boltzmann constant, h is the Planck's constant and T_p is the peak temperature of derivative curve of TGA.

The values of entropy gives information about the degree of order of the system, enthalpy gives information about the total thermal motion,

while Gibbs free energy gives idea about the stability of the system. The calculated values of E_a, enthalpy, entropy and Gibbs free energy of PF/ZnO-RGO nanocomposites were tabulated in Table 3. It is observed that the values of activation energies of the samples were changed indicating that the reinforcement of ZnO-RGO intensively affects the decomposition of the nanocomposites. From Table 3, it is clear that all parameters show irregular decrease. The positive value of ΔS is an indication of disorder in the reaction system. The calculated values of ΔG for all nanocomposites are negative and these are associated with spontaneity of reaction.

4. Conclusions

In the present work, we report the preparation of PF/ZnO-RGO nanocomposites by solution mixing method and investigated the structural, morphological, mechanical and thermal properties of nanocomposites. The XRD results confirmed the effective reinforcement of nanofillers into the PF matrix. TEM images gives information about the good dispersion state of the nanofillers in the PF matrix. Composites with 0.12 wt% of nanofiller showed better mechanical properties and it is due to the homogeneous dispersion of nanofillers in the PF matrix and strong interfacial interaction between polymer and naofillers. PF/ZnO-RGO nanocomposites with 0.12 wt% ZnO-RGO showed 54% increase in tensile strength and 107% increase in tensile modulus as compared to that of neat PF and it is due to the combined effect of ZnO nanoparticle and GO. SEM images of tensile fracture surface of nanofillers with good dispersion and aggregation showed a different morphology than that of neat PF. Izod impact strength of ZnO-RGO reinforced nanocomposites showed 47% increase as compared with that of neat PF. The influence of ZnO-RGO on the thermal stability and degradation kinetics of PF nanocomposites was investigated. The main weight loss was occurred in between 300 and 400 °C, due to the thermal decomposition of the polymeric chain. The thermal stability of PF/ZnO-RGO nanocomposites is not relevant to ZnO-RGO content but it is dependent on the dispersion of ZnO-RGO in the PF matrix. The thermal kinetic parameters such as activation energy, change in enthalpies, change in entropies and Gibb's functions were determined by Coats Redfern and Broido's method. The irregular changes produced in the activation energies of PF/ZnO-RGO nanocomposites showed that the addition of ZnO-RGO into the PF matrix intensively affects the decomposition of the nanocomposite. The values of thermodynamic parameters showed irregularity in the decomposition step with increase in the content of nanofiller. The low cost PF nanocomposites can be found multifunctional applications in various fields.

Author statement

All authors certify that they have participated sufficiently in the work to take public responsibility for the content, including participation in the concept, design, analysis, writing, or revision of the manuscript. Furthermore, each author certifies that this material or similar material has not been and will not be submitted to or published in any other publication before its appearance in the Diamond and Related Materials.

Declaration of competing interest

The authors declare that they have no known competing financial interests or personal relationships that could have appeared to influence the work reported in this paper.

Acknowledgements

The authors are grateful to the financial support under DST-FIST (No. 487/DST/FIST/15-16) New Delhi to Sree Sankara College, Kalady and Mahatma Gandhi University, Kottayam, India for the award of Junior Research Fellowship for Sandhya P K.

References

[1] Q. Lan, H. Shen, J. Li, C. Ren, X. Hu, Z. Yang, Facile synthesis of novel reduced graphene oxide@ polystyrene nanospheres for sensitive label-free electrochemical immunoassay, Chem. Commun. 56 (2020) 699–702.
[2] T.M. McCoy, G. Turpin, B.M. Teo, R.F. Tabor, Graphene oxide: surfactant or particle? Curr. Opin. Colloid Interface Sci. 39 (2019) 98–109.
[3] Y. Huang, T. Wang, X. Zhao, X. Wang, L. Zhou, Y. Yang, F. Liao, Y. Ju, Poly (lactic acid)/graphene oxide–ZnO nanocomposite films with good mechanical, dynamic mechanical, anti-UV and antibacterial properties, J. Chem. Technol. Biotechnol. 90 (2015) 1677–1684.
[4] S.S. Prasanna, K. Balaji, S. Pandey, S. Rana, Metal oxide based nanomaterials and their polymer nanocomposites, Nanomaterials and Polymer Nanocomposites, 2019, pp. 123–144.
[5] H. Moussa, E. Girot, K. Mozet, H. Alem, G. Medjahdi, R. Schneider, ZnO rods/reduced graphene oxide composites prepared via a solvothermal reaction for efficient sunlight-driven photocatalysis, Appl. Catal. B Environ. 185 (2016) 11–21.
[6] W.S. Solyman, H.M. Nagiub, N.A. Alian, N.O. Shaker, U.F. Kandil, Synthesis and characterization of phenol/formaldehyde nanocomposites: studying the effect of incorporating reactive rubber nanoparticles or Cloisite-30B nanoclay on the mechanical properties, morphology and thermal stability, J. Radiat. Res. Appl. Sci. 10 (2017) 72–79.
[7] D. Bansal, S. Pillay, U. Vaidya, Processing and characterization of nanographene platelets modified phenolic resin as a precursor to carbon/carbon composites (part II), J. Reinf. Plast. Compos. 32 (2013) 955–963.
[8] X.F. Wu, Y.K. Zhao, Y. Zhang, Y.Z. Wu, Y.J. Wang, H. Li, C.X. Zhang, X.Y. Yang, The comparison of mechanical and thermal properties of carbon nanotubes and graphene naonosheets enhanced phenol-formaldehyde resin, J. Chem. Soc. Pak. 39 (2017) 737.
[9] M.H. Choi, I.J. Chung, Mechanical and thermal properties of phenolic resin-layered silicate nanocomposites synthesized by melt intercalation, J. Appl. Polym. Sci. 90 (2003) 2316–2321.
[10] S. Wang, X. Jing, Y. Wang, J. Si, Synthesis and characterization of novel phenolic resins containing aryl-boron backbone and their utilization in polymeric composites with improved thermal and mechanical properties, Polym. Adv. Technol. 25 (2014) 152–159.
[11] Y. Guo, L. Hu, P. Jia, B. Zhang, Y. Zhou, Enhancement of thermal stability and chemical reactivity of phenolic resin ameliorated by nanoSiO_2, Korean J. Chem. Eng. 35 (2018) 298–302.
[12] M. Darwish, A. Mohammadi, N. Assi, Q.S. Manuchehri, Y. Alahmad, S. Abuzerr, Shape-controlled ZnO nanocrystals synthesized via auto combustion method and enhancement of the visible light catalytic activity by decoration on graphene, J. Alloys Compd. 703 (2017) 396–406.
[13] Z. Wu, L. Wang, Graphene oxide (GO) doping hexagonal flower-like ZnO as potential enhancer of photocatalytic ability, Mater. Lett. 234 (2019) 287–290.
[14] R. Banu, N. Salvi, C. Ameta, R. Ameta, P.B. Punjabi, Visible light driven photocatalytic degradation of brilliant green dye using graphene oxide/copper oxide binary composite, Indian J. Chem. 58 (2019) 157–166.
[15] T. Pisarkiewicz, L. Stobiński, W. Maziarz, D. Michoń, A. Malolepszy, A. Rydosz, Gas sensing properties of reduced graphene oxide modified by copper oxide, 2018 XV International Scientific Conference on Optoelectronic and Electronic Sensors (COE), 2018, pp. 1–3.
[16] E. Lee, D. Lee, J. Yoon, Y. Yin, Y.N. Lee, S. Uprety, Y.S. Yoon, D.J. Kim, Enhanced gas-sensing performance of GO/TiO2 composite by photocatalysis, Sensors 18 (2018) 3334.
[17] D. Zhang, X. Zhang, Q. Sun, S. Zheng, J. Hao, Y. Wang, Continuous photocatalysis based on layer-by-layer assembly of separation-free TiO2/reduced graphene oxide film catalysts with increased charge transfer and active site, Eur. J. Inorg. Chem. 2019 (2019) 721–729.
[18] W. Jihong, D. Ying, W. Yan, L. Qing, W. Hongyan, W. Qing, Adsorption of graphene on an Fe3O4 surface: a molecular dynamics simulation study, J. Adhes. 94 (2018) 238–253.
[19] S. Majumder, M. Sardar, B. Satpati, S. Kumar, S. Banerjee, Magnetization enhancement of Fe3O4 by attaching onto graphene oxide: an interfacial effect, J. Phys. Chem. C 122 (2018) 21356–21365.
[20] P. Li, Y. Zheng, M. Li, W. Fan, T. Shi, Y. Wang, A. Zhang, J. Wang, Enhanced flame-retardant property of epoxy composites filled with solvent-free and liquid-like graphene organic hybrid material decorated by zinc hydroxystannate boxes, Compos. A: Appl. Sci. Manuf. 81 (2016) 172–181.
[21] K. Deshmukh, M.B. Ahamed, R.R. Deshmukh, S.K. Pasha, K. Chidambaram, K.K. Sadasivuni, D. Ponnamma, M.A. AlMaadeed, Eco-friendly synthesis of graphene oxide reinforced hydroxypropyl methylcellulose/polyvinyl alcohol blend nanocomposites filled with zinc oxide nanoparticles for high-k capacitor applications, Polym.-Plast. Technol. Eng. 55 (2016) 1240–1253.
[22] P.K. Sandhya, J. Jose, M.S. Sreekala, M. Padmanabhan, N. Kalarikkal, S. Thomas, Reduced graphene oxide and ZnO decorated graphene for biomedical applications, Ceram. Int. 44 (2018) 15092–15098.
[23] E.N. Kalali, W. Guo, X. Wang, W. Xing, L. Song, Y. Hu, Effect of metal-based nanoparticles decorated graphene hybrids on flammability of epoxy nanocomposites, Compos. A: Appl. Sci. Manuf. 129 (2020) 105694.
[24] X. Zhao, Y. Li, J. Wang, Z. Ouyang, J. Li, G. Wei, Z. Su, Interactive

oxidation–reduction reaction for the in situ synthesis of graphene–phenol formaldehyde composites with enhanced properties, ACS Appl. Mater. Interfaces 6 (2014) 4254–4263.
[25] P.K. Sandhya, M.S. Sreekala, M. Padmanabhan, K. Jesitha, S. Thomas, Effect of starch reduced graphene oxide on thermal and mechanical properties of phenol formaldehyde resin nanocomposites, Compos. Part B 167 (2019) 83–92.
[26] S. He, Y. Qian, K. Liu, C.W. Macosko, A. Stein, Effects of inorganic fillers on toughening of vinyl ester resins by modified graphene oxide, Ind. Eng. Chem. Res. 57 (2018) 4592–4599.
[27] P. Krishnaiah, C.T. Ratnam, S. Manickam, Development of silane grafted halloysite nanotube reinforced polylactide nanocomposites for the enhancement of mechanical, thermal and dynamic-mechanical properties, Appl. Clay Sci. 135 (2017) 583–595.
[28] J. Si, J. Li, S. Wang, Y. Li, X. Jing, Enhanced thermal resistance of phenolic resin composites at low loading of graphene oxide, Compos. A: Appl. Sci. Manuf. 54 (2013) 166–172.
[29] M. Cui, S. Ren, S. Qin, Q. Xue, H. Zhao, L. Wang, Non-covalent functionalized hexagonal boron nitride nanoplatelets to improve corrosion and wear resistance of epoxy coatings, RSC Adv. 7 (2017) 44043–44053.
[30] S. Chhetri, N.C. Adak, P. Samanta, N.C. Murmu, D. Hui, T. Kuila, J.H. Lee, Investigation of the mechanical and thermal properties of l-glutathione modified graphene/epoxy composites, Compos. Part B 143 (2018) 105–112.
[31] S. Suresh, P. Nisha, P. Saravanan, K. Jayamoorthy, S. Karthikeyan, Investigation of the thermal and dielectric behavior of epoxy nano-hybrids by using silane modified nano-ZnO, Silicon 10 (2018) 1291–1303.
[32] L.H. Gaabour, Spectroscopic and thermal analysis of polyacrylamide/chitosan (PAM/CS) blend loaded by gold nanoparticles, Results Phys. 7 (2017) 2153–2158.